Konrad-Zuse-Zentrum
für Informationstechnik Berlin

Takustraße 7
D-14195 Berlin-Dahlem
Germany

MICHAEL OEVERMANN[1] HEIKO SCHMIDT[2]
ALAN R. KERSTEIN[3]

Linear-eddy modeling of autoignition under thermal stratification[4]

[1]Technische Universität Berlin, Institut für Energietechnik, e-mail: michael.oevermann@tu-berlin.de

[2]Zuse Institute Berlin (ZIB) and Freie Universität Berlin, Department of Mathematics and Computer Science, e-mail: heischmi@math.fu-berlin.de

[3]Combustion Research Facility, Sandia National Laboratories, Livermore, USA, e-mail: arkerst@sandia.gov

[4]Submitted to Combustion and Flame

The work was partially supported by DFG through grant SFB 557/B8 and by the Division of Chemical Sciences, Geosciences, and Biosciences, Office of Basic Energy Sciences, United States Department of Energy, and by the National Science Foundation under Grant No. ATM-0346854.

ZIB-Report 08-05 (Januar 2008)

Linear-eddy modeling of autoignition under thermal stratification[¶]

M. Oevermann, H. Schmidt, and A. R. Kerstein

January 31, 2008

Abstract

The influence of thermal stratification on autoignition at constant volume and high pressure is investigated under turbulent conditions using the one-dimensional Linear-Eddy Model (LEM) and detailed hydrogen/air chemistry. Results are presented for the influence of initial temperature inhomogeneities on the heat release rate and the relative importance of diffusion and chemical reactions. The predicted heat release rates are compared with heat release rates of Chen et al. [1] and Hawkes et al. [2] obtained by two-dimensional Direct Numerical Simulations (DNS). Using the definition of Chen et al. for the displacement speed of the H_2 mass fraction tracked at the location of maximum heat release, and a comparison of budget terms, different combustion modes including ignition front propagation and deflagration waves are identified and the results are compared to the DNS data. The LEM approach shows qualitatively and quantitatively reasonable agreement with the DNS data over the whole range of investigated temperature fluctuations. The results presented in this work suggest that LEM is a potential candidate as a sub-model for CFD calculations of HCCI engines.

Keywords: HCCI, autoignition, thermal explosion, turbulence, Linear-Eddy Model

[¶]Submitted to Combustion and Flame

Contents

1 Introduction

Homogeneous-charge compression ignition (HCCI) engines have potentially higher thermal efficiencies and lower NO_x and soot emissions compared to conventional spark-ignition and Diesel engines, respectively. Compared to conventional compression-ignition (CI) engines, HCCI engines operate under lean conditions with fuel and air well mixed before entering the cylinder. Although major progress has been made, HCCI engines suffer from high carbon monoxide (CO) and unburned hydrocarbon (UHC) emissions. In order to achieve low NO_x emissions HCCI engines usually operate with very lean fuel/air mixtures and/or exhaust gas recirculation (ECR) to keep peak temperatures low. However, such low temperature levels will favor incomplete combustion and high CO levels. Another major problem in the design of HCCI engines is the control of the very large heat release rates which may cause excessively rapid pressure rise under perfectly homogeneous conditions. One method to reduce the maximum heat release rate is the introduction of thermal or mixture inhomogeneities. Temperature inhomogeneities will lead to some hot and some cold spots each having different ignition delay times. The hottest spots will ignite first followed by the colder areas leading to a spreading of the heat release over several crank angles. Ignited and un-ignited spots build up large temperature gradients between burned and unburned gas where turbulent and molecular mixing become important and cannot be neglected.

In recent Direct Numerical Simulation (DNS) studies [1, 2] it has been demonstrated that both ignition fronts and deflagration-like fronts may be present under thermal stratification under HCCI-like conditions. With increasing stratification the subtle interaction between turbulent mixing and chemistry becomes increasingly important and needs to be taken into account in computational models of HCCI engines. Cook et al. [3] presented a one-dimensional flamelet-type model in enthalpy space capable of capturing HCCI combustion in both relevant regimes identified in the DNS simulation. The model offers the potential to be used as a combustion model for CFD calculations of HCCI engines. However, for closure the enthalpy-based flamelet model needs a probability density function (PDF) for enthalpy and a model for the enthalpy dissipation rate. Using those data directly from the DNS [3], the enthalpy flamelet model was able to achieve good agreement with the DNS results.

Steeper et al. [4] applied the Linear-Eddy Model as a stand alone tool for the investigation of spatial fuel distribution under typical HCCI conditions. They used a simple two-step, six-species chemical mechanism for n-heptane which was not able to capture the characteristic low temperature heat release of n-heptane. The authors presented some interesting qualitative results with the LEM, however they did not make any quantitative comparison with experimental data or other numerical modeling appoaches.

In this work we use the Linear-Eddy Model (LEM) [5] to investigate the influence of thermal stratification on auto-ignition under HCCI conditions and compare the results with recent DNS data of Hawkes et al. [1, 2]. The (one-dimensional) LEM is capable of representing the turbulence-chemistry interaction at all temporal and spatial scales. In comparison to the flamelet-based modeling of Cook at al. [3] the LEM approach after calibration does not need additional input for closure. The predicted heat release rates and the relative importance of reaction and diffusion terms agree reasonably well with the DNS results.

The simple one-dimensional model is capable of capturing the key combustion characteristics for the combustion regime of spontaneous ignition fronts, for the deflagration-dominated case, and lastly for the mixed one. The 1D strategy enables parametric studies, including modification of mixture inhomogeneity, in a reasonable computational time. Furthermore, LEM has been used successfully in the past as a subgrid combustion model for Large Eddy Simulations, e. g. [6, 7, 8]. The results presented in this work suggest that LEM is a potential candidate as a sub-model for CFD calculations of HCCI engines.

The paper is organized as follows: In the next Section we introduce our modeling strategy using LEM. In Section 3 we compare results obtainced with the LEM approach with some recent DNS data and finish in Section 4 with some concluding remarks.

2 Model formulation

The Linear-Eddy Model was proposed by Kerstein in [5] for non-reacting flow and extended to reactive flow in [9]. It has been discussed in detail in the literature, e.g. [5, 9, 10, 11, 12] and, therefore, is only briefly summarized here. The overall LEM concept for turbulent reactive flow consists of two concurrent processes representing the respective influences of dilatation-induced advection, molecular diffusion, chemical reactions and turbulent transport. The first process is time advancement of the reactive zero-Mach-number equations on a one-dimensional domain resolving all spatial and temporal scales. The second process, turbulent transport, is implemented using a stochastic sequence of statistically independent stirring events.

2.1 The zero-Mach-number equations for reactive flow

We solve the variable density zero-Mach-number equations in one spatial dimension on a fixed grid. The balance equations for species mass fractions and temperature are

$$\rho\frac{\partial Y_s}{\partial t} + \rho u\,\frac{\partial Y_s}{\partial x} = -\frac{\partial j_s}{\partial x} + M_s\,\dot{\omega}_s, \tag{1}$$

$$\rho c_p\frac{\partial T}{\partial t} + \rho u c_p\,\frac{\partial T}{\partial x} = \frac{\mathrm{d}p}{\mathrm{d}t} - \frac{\partial q}{\partial x} - \sum_s j_s\,\frac{\partial h_s}{\partial x} - \sum_s h_s\,M_s\,\dot{\omega}_s, \tag{2}$$

with $s = 1, \ldots, n_s$ and n_s is the number of different species in the system. Here, ρ is the density, Y_s the mass fraction of species s, u the velocity, j_s the species diffusive flux, M_s the molecular weight of species s, $\dot{\omega}_s$ the chemical source term of species s, c_p the heat capacity at constant pressure, p the pressure, q the heat flux, and h_s the enthalpy of species s including the heats of formation. For the equation of state of a mixture of ideal gases we have

$$p = \rho T \sum_s Y_s R_s, \tag{3}$$

with R_s denoting the individual gas constant of species s.

In the zero-Mach-number limit the thermodynamic pressure p is spatially constant [13]. In this case a divergence constraint on the velocity can be derived from the energy equation [14]:

$$\frac{\partial u}{\partial x} = -\frac{1}{\gamma\, p}\frac{\mathrm{d}p}{\mathrm{d}t} + \mathcal{U}, \tag{4}$$

where γ is the ratio of specific heats and $\mathcal{U}$ is given by

$$\begin{aligned}\mathcal{U} = &-\frac{1}{\rho c_p T}\left\{\frac{\partial q}{\partial x} + \sum_s j_s \frac{\partial h_s}{\partial x}\right\} \\ &-\frac{1}{\rho}\sum_s \left\{\frac{M}{M_s}\frac{\partial j_s}{\partial x}\right\} + \frac{1}{\rho}\sum_s \left\{\frac{M}{M_s} - \frac{h_s}{c_p T}\right\}\dot{\sigma}_s.\end{aligned}$$

Here M denotes the mean molecular weight of the mixture and $\dot{\sigma}_s = M_s\,\dot{\omega}_s$. Integrating (4) over the whole domain from $x = x_1$ to $x = x_1 + L$ results in an equation for the global pressure change

$$\frac{\mathrm{d}p}{\mathrm{d}t} = \frac{\gamma\, p}{L}\left\{\int_{x=x_1}^{x_1+L} \mathcal{U}\,\mathrm{d}x - (u_2 - u_1)\right\}. \tag{5}$$

For periodic or zero-velocity boundary conditions we have $u_1 = u_2$ and the last term in (5) vanishes. In these conditions (the latter is used here, see Section 2.3) equation (5) allows us to calculate the pressure rise due to chemical reactions, heat conduction, and species diffusion. In the one-dimensional case equation (4) allows the computation of the velocity by simple integration in space. Therefore it is not necessary to solve a momentum equation here. The velocity u in eq. (1), (2), and (4) represents the flow velocity induced by dilatational effects due to compression, conduction, and chemical reactions as given by (4).

It is important to note that similar to a DNS, in the LEM concept equations (1) and (2) need to resolve all spatial scales of a turbulent reacting flow.

2.2 Linear eddy mixing / turbulent transport

In the LEM concept, turbulent advection is implemented explicitly by stochastic eddy events. Each eddy event involves a rearrangement of all scalar quantities using so-called 'triplet maps.' The effect of a triplet map is a three-fold compression of the scalar fields in a selected spatial interval whose size is denoted by l. This map increases the scalar gradients within the selected interval, analogous to the effect of compressive strain in turbulent flow, without creating discontinuities.

Two quantities are needed to specify an eddy event: eddy size l and eddy location within the domain. The eddy location is randomly sampled from a uniform distribution, and the eddy size is randomly sampled. Assuming the Kolmogorov inertial-range scaling the size distribution is given by [5]

$$f(l) = (5/3)\; l^{-8/3}/[\eta^{-5/3} - l_t^{-5/3}].$$

Using the turbulent Reynolds number

$$Re_t = \frac{u' l_t}{\nu},$$

where ν is the kinematic viscosity, and u', l_t are the integral velocity and length scale, respectively, the Kolmogorov scale η is determined from the inertial scaling law

$$\eta = N_\eta \, l_t \, Re_t^{-3/4}.$$

Here, N_η is an empirical constant.

Eddy events induce a random walk of fluid parcels whose diffusivity is the model analog to the turbulent diffusivity D_t. Based on this interpretation, the event frequency per unit length is determined by [5]

$$\lambda = \frac{54}{5} \frac{\nu Re_t}{C_\lambda l_t^3} \frac{\left[(l_t/\eta)^{5/3} - 1\right]}{\left[1 - (\eta/l_t)^{4/3}\right]}.$$

The required model constants have been set to $C_\lambda = 15$ and $N_\eta = 10$. The value for C_λ has been adopted from [15]. Out of a few iterations with different values for N_η this parameter set gave the best agreement with DNS data. More careful tuning might lead to a further improvement of the results. However, it should be pointed out that this tuning of parameters needs to be done only once for some model configuration. Once a suitable parameter set has been determined, the model should be applicable for any other operating conditions.

2.3 Numerical implementation

The zero-Mach-number equations are solved numerically using standard second-order finite-difference discretization. No-flux boundary conditions are applied hence $u_1 = u_2 = 0$. Periodic boundary conditions, consistent with the DNS comparison case, will be applied in the future. Results thus far indicate that this change will have negligible effect, especially for those cases where we use a LEM domain size much larger than the size of the DNS domain, see Section 3.3.

The time integration of the stiff set of equations is performed using the DAE solver IDA of the SUNDIALS package [16]. In order to not destroy the bandstructure of the sparse solver, no-flux boundary conditions are applied for all variables. Periodic boundary conditions, consistent with the DNS comparison case, would require major changes in the IDA solver. However, as the LEM simulations are performed on a much larger spatial domain than the DNS, the use of no-flux instead of periodic boundary conditions can safely be assumed to have a negligible effect here.

Thermodynamic and transport properties as well as reaction rates are calculated using the C++ interface of the CANTERA software package [17].

3 Results

3.1 Initial conditions

We test the LEM approach against DNS results presented in [2]. The equivalence ratio of the initially homogeneous H_2-air mixture is $\phi = 0.1$ in all cases. Initial pressure and temperature are $p_0 = 41$ atm and $T_0 = 1070$ K, respectively. The calculated ignition delay time for a homogeneous mixture under these conditions is $t_{ig} = 2.9$ ms. The detailed chemical mechanism for H_2-air

chemistry has been taken from [18] and uses 8 reactive species (see Table 1) and 21 reversible reactions. The initial conditions correspond to a compression ratio of 15:1 starting at 1 atm and 400K. Decoupling the compression stage from the ignition stage is justifiable for hydrogen/air chemistry which exhibits very low heat release rates at lower temperatures. However, such an approximation is inadequate for more realistic fuels such as n-heptane with multistage ignition behavior. These parameters have been argued in [2] to be representative for engines operating at low load. Due to the relatively low equivalence ratio and the moderate compression rate it can be safely assumed that developing compressive waves such as shocks and detonations are not present [2].

Integral turbulent length and velocity scales for the LEM runs are taken from the DNS and are $l_t = 0.34$ mm and $u' = 0.5$ m/s. A random temperature field with a Passot-Pouquet spectrum [19]

$$E(k) = \frac{32}{3}\sqrt{\frac{2}{\pi}}\frac{T'^2}{k_e}\left(\frac{k}{k_e}\right)^4 \exp\left(-2\left(\frac{k}{k_e}\right)^2\right) \tag{6}$$

is superimposed on the mean temperature field to specify initial temperature inhomogeneities. Here, k is the wave number, k_e is the most energetic wave number defined by $k_e = 2\pi/l_e$, and T' is the RMS temperature fluctuation.

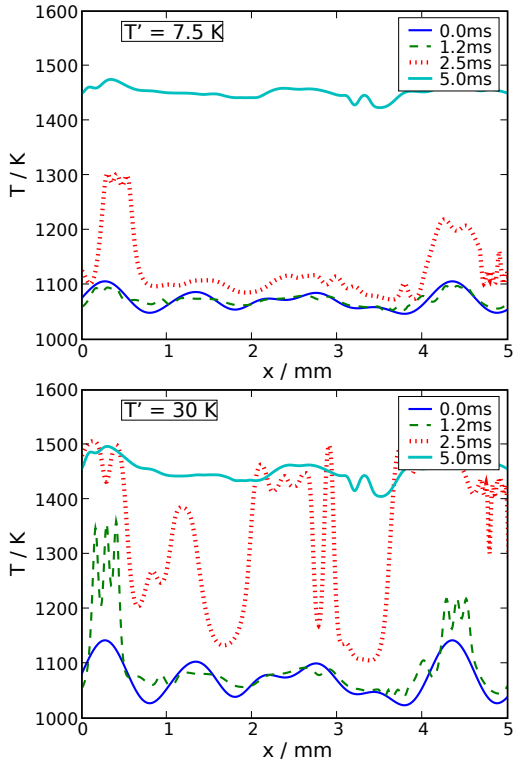

Figure 1: Temperature profiles at different times for initial temperature RMS values of $T' = 7.5$ K and 30 K.

	H_2	O_2	O	OH	H_2O	H	HO_2	H_2O_2	N_2
Le_s	0.32	1.15	0.75	0.76	0.84	0.19	1.16	1.16	1.00

Table 1: Lewis numbers for all species

The resulting initial temperature field is

$$T(x) = T_0 + \sum_{k=1}^{\infty} (\Delta T)_k \, \sin\left(2\pi \, k \, x/L + \phi_k\right), \tag{7}$$

where T_0 denotes the initial mean temperature, and ϕ_k is the randomly chosen phase of mode k with $0 \leq \phi_k \leq 2\pi$. The temperature amplitude at wavenumber k for a periodic temperature field with a discrete spectrum is given by

$$(\Delta T)_k = \left(2 \int_{k-1/2}^{k+1/2} E(k) \, \mathrm{d}k\right)^{1/2} \approx \left(2 \, E(k)\right)^{1/2}.$$

With this initialisation the resulting initial temperature field has exactly the prescribed RMS value T'.

In accordance with the DNS, the most energetic length scale is $l_e = 1.32$ mm. The initial velocity RMS is $v' = 0.5$ m/s and the initial autocorrelation integral length scale is $l_t = 0.34$ mm. This leads to a turbulent Reynolds-number of $Re_t = 45$. The characteristic integral time scale can be estimated by $t_t = l_t/v' = 0.68$ ms which is of the same order of magnitude as the homogeneous ignition delay time $t_{ig} = 2.9$ ms and therefore allows for strong interactions between turbulence and chemistry.

The diffusion coefficients are calculated in accordance with the DNS from the prescribed Lewis numbers shown in Table 1. Transport coefficients are evaluated as mixture avaraged values and all thermodynamic quantities are evaluated from the well known NASA polynomials using CANTERA's built-in routines.

All LEM simulations in this study have been run with a uniform grid spacing of 4.3 μm taken from the DNS. This grid spacing has been reported in [1] to be necessary and sufficient to resolve ignition fronts under the given conditions.

3.2 Spatial structure of ignition

For a qualitative picture of the spatial structure of a typical ignition event, Figure 1 shows temperature profiles at different times for $T' = 7.5$ K and 30 K. The low fluctuations in the first case lead to an almost homogeneous auto ignition with only two moderate hot spots advancing ahead of an almost homogeneous region in between. From the $T' = 30$ K case it becomes obvious that the large initial temperature fluctuations induce locally different ignition delays between initial minimum and maximum values resulting in large temperature gradients. These temperature gradients are subject to turbulent mixing during the 'delay time window'.

3.3 Domain size influence

In order to get meaningful statistics within the LEM approach it is necessary to either perform many different realizations on a LEM domain with a linear

dimension comparable to the DNS, or to run a single calculation on a domain much larger than the spatial extent of the two-dimensional DNS of Chen [1], which is $l_{DNS} \times l_{DNS}$ with $l_{DNS} = 4.1$ mm. Here we follow the second approach. Figure 2 shows heat release rates as a function of time for different random initial temperature distributions. Time and heat release rates have been made non-dimensional by the ignition delay time and the peak heat release rate of the homogeneous reactor, respectively. In the top graph of Figure 2 the LEM domain is $l_{LEM} = l_{DNS}$ corresponding exactly to the spatial extent of the DNS. It is obvious that different initial conditions lead to very different heat release rates over time. The bottom graph of that figure shows heat release rates with five different random initial conditions with a spatial domain $l_{LEM} = 50\, l_{DNS}$. Each calculation can be interpreted as a representation of 50 different realizations of initial conditions with $l_{LEM} = l_{DNS}$. We note that different random seeds have been used in each calculation for implementation of the LEM stirring events. Based on the heat release rates versus time and the small deviations between the five different calculations we suppose that 50 realizations or an LEM domain of 50 times the DNS domain size give reasonable statistical results for this study. All results presented below use a LEM domain $l_{LEM} = 50\, l_{DNS}$.

3.4 Heat release rates

The principal influence of initial temperature fluctuations and turbulent mixing is shown in Figure 3. During the initial ignition stage the influence of turbulence is almost negligible. However, during the phase of peak heat release turbulence cannot be neglected. In all cases turbulence leads to increased peak heat release rates. This is due to the fact that turbulence tends to homogenize the initial

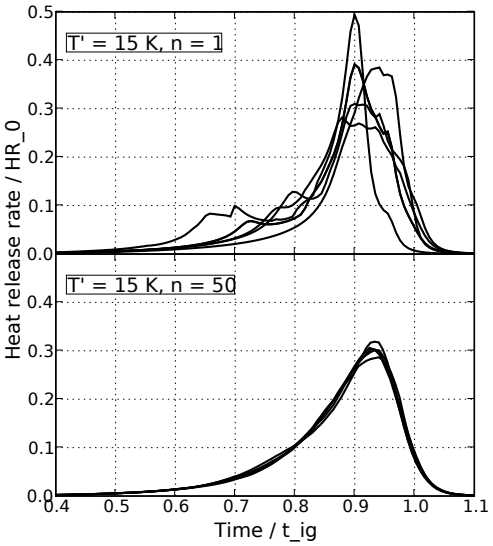

Figure 2: Influence of LEM domain size on heat release rates. $l_{LEM} = n\, l_{DNS}$

temperature fluctuations bringing heat release rates closer to the homogeneous reactor case with its typical explosion behaviour for reactions with high activation energy. Figure 3 shows that both initial temperature fluctuations and turbulent mixing have a distinct influence on heat release rates under HCCI conditions.

Figure 4 shows heat release rates over time for different T' values. With increasing T', the heat release is spread over a longer time period. Reasonable agreement is obtained between the DNS results of Hawkes et al. [2] and LEM for temperature fluctuations $T' = 3.75$ K, 7.5 K, and 15 K, although less so as T' increases.

Besides the obvious conceptual differences between the one-dimensional LEM and the two-dimensional DNS there are some other important differences here. Whereas the DNS represents decaying turbulence, the LEM as implemented here mimics a constant turbulence level. The tuning of N_η described in Sec. 2.2 enforces overall conformance of LEM to DNS mixing properties. For present purposes, it is not necessary to match mixing properties in finer detail, but it could be useful in future studies. In addition, LEM is formulated to represent the 3D inertial-range cascade (Section 2.2 and cited references), but 2D DNS has different cascade physics and scalings. Finally, the LEM calculations with a domain size of $l_{LEM} = 50\, l_{DNS}$ can be – to a certain degree, see Section 3.3 – regarded as statistically convergent whereas each DNS result corresponds to a single representation of the process. Despite these differences between models, the LEM is able to produce heat release rates which are qualitatively and quantitatively comparable to DNS results.

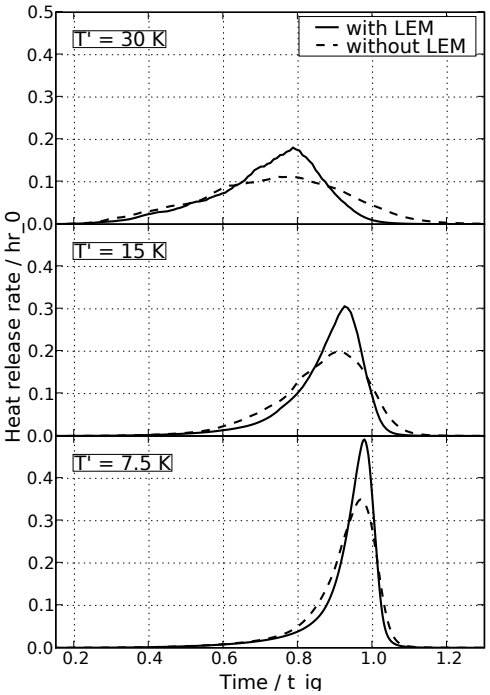

Figure 3: Influence of turbulence on heat release rates

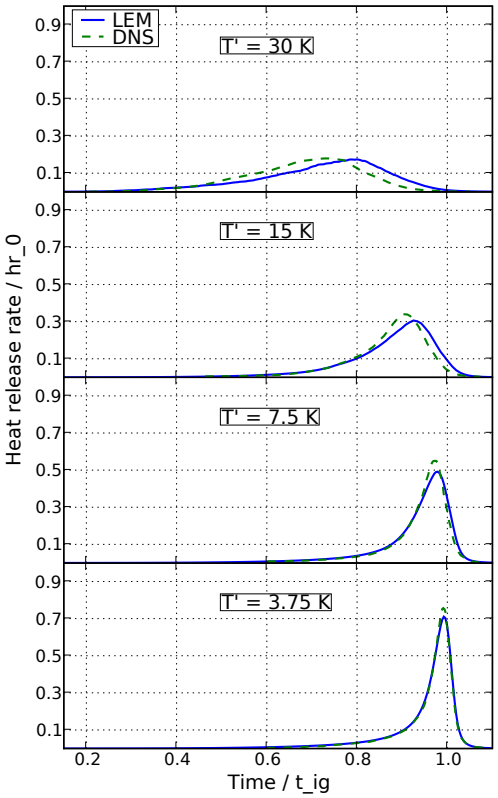

Figure 4: Heat release versus time for different initial temperature fluctuations.

3.5 Mean reaction front speed

Zel'dovich [20] distinguished five different combustion modes in a homogeneous mixture with a non-homogeneous initial temperature distribution: (i) near instantaneous thermal explosions, (ii) conventional deflagration waves, (iii) developing detonation waves, (iv) subsonic, and (v) supersonic autoignitive spontaneous ignition fronts driven by a non-uniform distribution of ignition delay times corresponding to temperature inhomogeneities. These different regimes have been identified in [21] by comparing the initial temperature gradient to the critical temperature gradient of a hot spot leading to a sonic reaction front speed.

A definition for a density weighted displacement speed capable of representing all regimes between the spontaneous ignition front propagation (where molecular transport is negligible) and the deflagration wave has been derived in [22]. In one spatial dimension this displacement speed is given by the density weighted material derivative of a scalar ϕ at a fixed value $\phi^\star$

$$s_d^\star = \frac{\rho}{\rho_u} \frac{\mathrm{D}\phi^\star}{\mathrm{D}t} \left(\frac{\mathrm{d}\phi}{\mathrm{d}x} \right)^{-1}_{\phi=\phi^\star},$$

where ρ_u is a representative density of the reactants at the local conditions which can be calculated from the local enthalpy and the unburned mixture composition assuming constant pressure. With $\phi = Y_{\mathrm{H}_2}$ and replacing the material derivative with the transport equation for the species mass fraction (1) we can write

$$s_d^\star = -\frac{1}{\rho_u} \left\{ \frac{\mathrm{d}j_{\mathrm{H}_2}}{\mathrm{d}x} - M_{\mathrm{H}_2}\, \dot{\omega}_{\mathrm{H}_2} \right\} \left(\frac{\mathrm{d}Y_{\mathrm{H}_2}}{\mathrm{d}x} \right)^{-1}_{Y_{\mathrm{H}_2}=Y^\star_{\mathrm{H}_2}}. \tag{8}$$

For a steady planar deflagration wave without heat loss the density weighted displacement speed is constant over the flame structure. This definition has been used in the DNS study [1, 2] as an indicator for identifying different combustion regimes and will be used here as well. As a reference value for tracking the front a value of $Y_{\mathrm{H}_2^\star} = 8.5 \times 10^{-4}$ has been used [1]. This value corresponds approximately to the value at maximum heat release.

Figure 5 shows displacement speeds over time for different initial temperature fluctuations and compares LEM results with DNS results taken from [2]. We remark that the LEM displacement speeds shown in Figure 5 are arithmetic mean values of all displacement speeds at a given time observed within the LEM domain. The LEM calculations show the same qualitative U shape as the DNS. The minimum speed decreases with increasing temperature fluctuations T' and the quantitative values obtained with the LEM model and the DNS are of the same order of magnitude. Because LEM values are averages over individual, separately propagating reaction zones but DNS values are averages over smooth iso-contours, LEM results are more intermittent than the DNS. The laminar flame speed under the local conditions are in the order of 40-50 cm/s, see Figure 3 of [1]. From Figure 5 it becomes obvious that the observed displacement speed for the $T' = 30\ K$ is mostly in the vicinity of the laminar flame speed, indicating the importance of both reaction and diffusion in this regime. With decreasing temperature fluctuations the observed displacement speeds increase in accordance with the expectation that with decreasing molecular transport the front speed increases towards the displacement speeds of the spontaneous ignition front propagation.

3.6 Budget terms

The relative importance of diffusion and the chemical source term for hydrogen mass fraction is shown in Figure 6 for an initial temperature fluctuation of $T' = 15$ K. Consistent with the heat releases rates for the $T' = 15$ K case in Figure 4 the profiles of the LEM simulation lag in time behind the DNS data with a slightly lower peak reaction term in the LEM simulation. The DNS data are taken from Figure 15 of [1] and for the diffusion term the absolute value has been taken for comparison. Again, the overall agreement between the LEM and the DNS is quite reasonable here. At peak heat release the H_2 reaction term equals $5.71\,\mathrm{s}^{-1}$ and the diffusion term $1.54\,\mathrm{s}^{-1}$ which corresponds to 27% of the source term. This value is in excellent agreement with the DNS value of 27% reported in [1].

Whereas Figure 6 shows a quantitative comparison of spatially averaged H_2 reaction and diffusion budget terms between LEM and DNS, Figure 7 shows the budget terms for different initial temperature fluctuations. For $T' = 3.75\,K$ the molecular diffusion term is negligible compared to the chemical source term. With increasing initial temperature fluctuations the relative importance of the diffuson term increases. At T' the diffusion and source terms are the same order of magnitude, which is typical for propagating flame fronts. In accordance with the discussion given in Section 3.5, Figure 7 indicates different combustion modes ranging from ignition front propagation to deflagration-like combustion waves.

Another indicator for different combustion modes under HCCI conditions

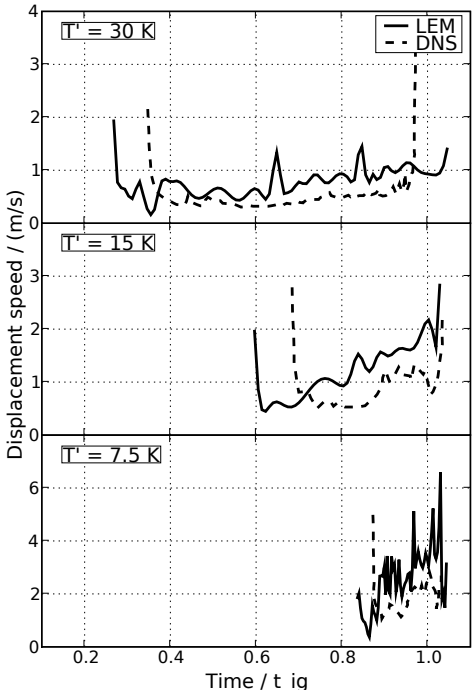

Figure 5: Displacement speed over time for the LEM and DNS.

can obtained from the PDF of the ratio of diffusion and reaction budget terms. In [3], PDFs of this ratio based on the DNS of [2] have been presented. Figure 8 shows the corresponding PDFs for the LEM. In accordance with [2] the PDFs have been computed at the time of maximum heat release and an isolevel $Y_{H_2} = 0.00033$. From Figure 8 it can be observed that with increasing initial

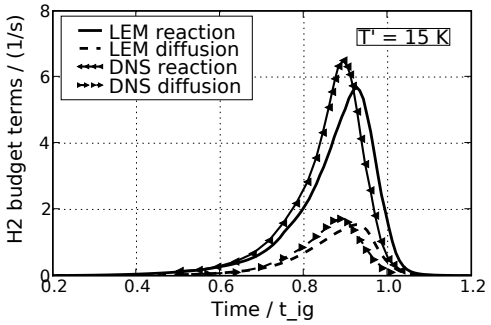

Figure 6: DNS and LEM spatially averaged H_2 diffusion and reaction budget terms.

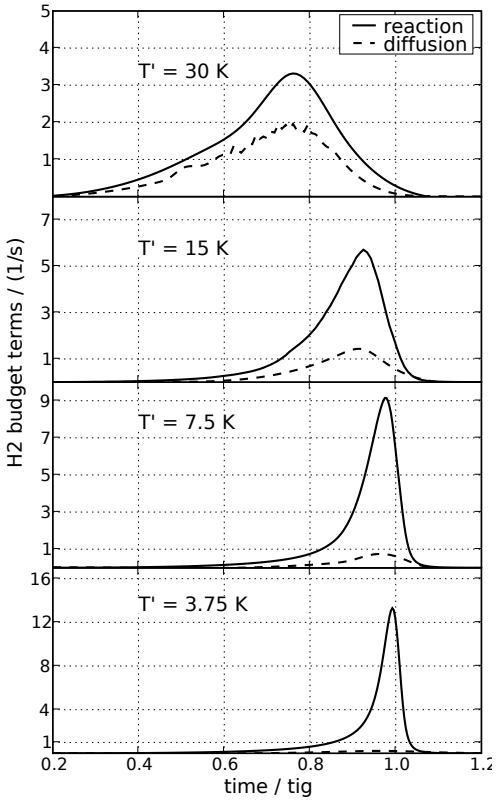

Figure 7: LEM spatially averaged H_2 diffusion and reaction budget terms.

temperature fluctuations the PDFs becomes broader indicating the increased importance of the diffusion relative to the chemical source term. For $T' = 3.75\,K$ the PDF shows a narrow profile with a peak value at zero budget ratio corresponding to negligible diffusion in this case. For $T' = 30\,K$ the PDF has a broad profile for budget ratios up to approximately 0.7. Despite some quantitative differences between the LEM PDF in Figure 8 and the DNS PDF presented in [3] some key features of the DNS PDFs are reproduced by the LEM: A monotonic decrease of the PDF for $T' = 3.75\,\mathrm{K}$ and $7.5\,\mathrm{K}$, a shoulder that extends to about 0.5 (about 0.6 in the DNS) for $T' = 15\,\mathrm{K}$, and a slight upward trend peaking at about 0.7 for $T' = 30\,\mathrm{K}$. These results further illustrate the progression, with increasing T', from ignition front propagation, through a mixed regime, and then toward deflagration-like combustion in the LEM simulations as well as the DNS.

4 Conclusions

We have presented an application of the Linear-Eddy Model for the simulation of autoignition under thermal stratification under HCCI conditions. A detailed hydrogen chemical mechanism has been used. We compared LEM results with recent DNS data. The predicted heat release rates as well as the relative importance of reaction and diffusion terms agree qualitatively and quantitatively reasonably well with the DNS results. The simple one-dimensional LEM model is capable of capturing the key combustion characteristics for the combustion regime of spontaneous ignition fronts, for the deflagration dominated case, and lastly for the mixed one.

The comparisons to DNS do not constitute a validation of the LEM simulations because the DNS, being 2D, is itself a model rather than a quantitatively accurate flow simulation. The relationship between the two methods is that they both advance the spatially and temporally resolved diffusion and reaction processes and both involve idealized (relative to 3D turbulence) representations of advection, where the nature of the idealization is different in the two methods. The consistency of the results obtained using the two methods suggests that the

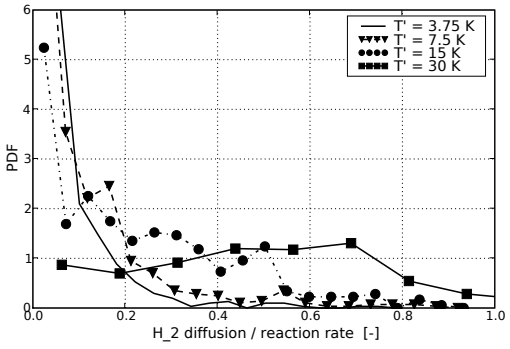

Figure 8: PDF of the diffusion to reaction budget term ratio for the H_2 mass fraction constrained to the peak heat release and a value of $Y_{H_2} = 0.00033$.

salient features of the combustion regime considered here are insensitive to the details of advection modeling.

The 1D strategy of LEM enables parametric studies including modification of mixture inhomogeneity in a reasonable computational time. Despite the limitations of being 1D only, it is especially this feature that allows the investigation of turbulent Reynolds numbers regimes which are not accessible by 2D or 3D DNS. The results presented in this work suggest that LEM is a potential candidate as a sub-model for CFD calculations of HCCI engines.

Acknowledgments

The authors acknowledge the support and helpful discussions with J. Chen and E. Hawkes.

This work was partially supported by the Division of Chemical Sciences, Geosciences, and Biosciences, Office of Basic Energy Sciences, United States Department of Energy, and by the National Science Foundation under Grant No. ATM-0346854. Sandia National Laboratories is a multi-program laboratory operated by Sandia Corporation, a Lockheed Martin Company, for the United States Department of Energy under contract DE-AC04-94-AL85000.

References

[1] J. H. Chen, E. R. Hawkes, R. Sankaran, S. D. Scott, H. G. Im, Direct numerical simulation of ignition front propagation in a constant volume with temperature inhomogeneities I. Fundamental analysis and diagnostics, Combustion and Flame 145 (2006) 128–144.

[2] E. R. Hawkes, R. Sankaran, P. P. Pébay, J. H. Chen, Direct numerical simulation of ignition front propagation in a constant volume with temperature inhomogeneities II. Parametric study, Combustion and Flame 145 (2006) 145–159.

[3] D. J. Cook, H. Pitsch, J. H. Chen, E. R. Hawkes, Flamelet-based modeling of auto-ignition with thermal inhomogeneities for application to HCCI engines, Proceedings of the Combustion Institute 30 (2006) 2903–2911.

[4] R. Steeper, V. Sankaran, J. Oefelein, Simulation of the effect of spatial fuel distribution using a linear-eddy model, SAE Technical Paper Series 2007-01-4131.

[5] A. R. Kerstein, Linear-eddy model of turbulent transport. 2. Application to shear-layer mixing, Combustion and Flame 75 (1989) 397–413.

[6] V. K. Chakravarthy, S. Menon, Subgrid modeling of turbulent premixed flames in the flamelet regime, Flow, Turbulence and Combustion 65 (2000) 133–161.

[7] V. K. Chakravarthy, S. Menon, Subgrid modeling of turbulent premixed flames in the flamelet regime, Combustion Science and Technology 162 (2001) 175–222.

[8] V. Sankaran, S. Menon, Subgrid combustion modeling of 3-d premixed flames in the thin-reaction-zone regime, Proceedings of the Combustion Institute 30 (2005) 575–582.

[9] A. R. Kerstein, Linear-eddy model of turbulent transport. Part 4. Structure of diffusion flames, Combustion Science and Technology 81 (1992) 75–96.

[10] A. R. Kerstein, A linear-eddy model of turbulent scalar transport and mixing, Combustion Science and Technology 60 (1988) 391–421.

[11] A. R. Kerstein, Linear-eddy modeling of turbulent transport. Part 6. Microstrcture of diffisive scalar mixing, Journal of Fluid Mechanics 231 (1991) 361–394.

[12] A. R. Kerstein, Linear-eddy model of turbulent transport. Part 7. Finite-rate chemistry and multi-stream mixing, Journal of Fluid Mechanics 240 (1992) 289–313.

[13] R. Klein, Semi-Implicit Extension of a Godunov-Type Scheme Based on Low Mach Number Asymptotics I: One-Dimensional Flow, Journal of Computational Physics 121 (1995) 213–237.

[14] M. S. Day, J. B. Bell, Numerical simulation of laminar reacting flows with complex chemistry, Combustion Theory and Modeling (4) (2000) 535–556.

[15] V. Sankaran, S. Menon, Structure of premixed turbulent flames in the thin-reaction-zones regime, Proceedings of the Combustion Institute 28 (2000) 203–209.

[16] A. C. Hindmarsh, Sundials: Suite of nonlinear and differential/algebraic equation solvers, Tech. Rep. UCRL-JRNL-200037, Lawrence Livermore National Laboratory (2004).

[17] D. Goodwin, Cantera: Object-oriented software for reacting flows. `http://www.cantera.org`.

[18] M. A. Mueller, T. J. Kim, R. A. Yetter, F. L. Dryer, Flow reactor studies and kinetic modeling of the H_2/O_2 reaction, Int. J. Chem. Kinet. 31 (1999) 113–125.

[19] J. O. Hinze, Turbulence, McGraw-Hill, 1975.

[20] Y. B. Zel'dovich, Regime classification of an exothermic reaction with nonuniform initial conditions, Combustion and Flame 39 (1980) 211–214.

[21] X. J. Gu, D. R. Emerson, D. Bradley, Modes of reaction front propagation from hot spots, Combustion and Flame 133 (2003) 63–74.

[22] T. Echekki, J. H. Chen, Analysis of the contribution of curvature to premixed flame propagation, Combustion and Flame 118 (1999) 308–311.